Atmos. Chem. Phys. Discuss.,
https://doi.org/10.5194/acp-2018-1312-AC1, 2020

Atmospheric Chemistry and Physics Discussions

Interactive comment on "Tropical Pacific Climate Variability under Solar Geoengineering: Impacts on ENSO Extremes" *by* Abdul Malik et al.

Abdul Malik et al.

abdul.malik@kaust.edu.sa

Received and published: 29 August 2020

Major Points

1)

It is not clear exactly why the modeled ENSO changed from 4xCO2 to G1 in this model? Is it because of the air-sea heat fluxes act more less as a damping in the eastern equatorial Pacific associated with the mean state change in G1? More interestingly, why G1 does not recover many of the climatic states of piControl? Initial thought would be the ocean state never fully recovers. But as stated in the paper the change in thermocline depth is not statistically different between G1 and piControl. I don't think I came across a plot of subsurface temperature, e.g., depth-longitude differences between 4xCO2

and G1 vs piControl. Perhaps while the thermocline depth statistics do not change, there are still changes in the subsurface ocean temperatures in certain areas.

Reply:

In the revised manuscript, we have calculated ENSO feedbacks, Bjerknes and heat flux, and ocean stratification to explain the mechanisms for change in ENSO. We have added Section 4 elaborating on the mechanism for change in ENSO under both 4xCO2 and G1. (See section 4, from page 17 and line 1 to page 18 and line 29). Specifically we write:

4 Mechanisms behind the changes in ENSO variability

4.1 Under greenhouse gas forcing

The reduced ENSO amplitude under 4×CO2 is mainly caused by stronger hf and weaker BJ feedback relative to piControl (Fig. 15a-b, and Table S5-6). More rapid warming over the eastern than western equatorial Pacific regions reduces the SST asymmetry between western and eastern Pacific (Fig. 1d), resulting in the weakening of ZSSTG (Fig. 4b) that significantly weakens the zonal winds stress (Fig. 4a) and hence PWC (Fig. 6b, d, see Bayr et al., 2014). The overall reduction of zonal wind stress reduces the BJ feedback, which, in turn, can weaken the ENSO amplitude. Climate models show an inverse relationship between hf feedback and ENSO amplitude (Lloyd et al., 2009, 2011; Kim and Jin 2011b). The increased hf feedback might be the result of enhanced clouds due to strengthened convection (Fig. 5b, d) and stronger evaporative cooling in response to enhanced SSTs under 4×CO2 (Knutson and Manabe 1994; Kim and Jin 2011b). Kim and Jin (2011a, b) found intermodel consensus on the strengthening of hf feedback in CMIP3 models under enhanced GHG warming scenario (Ferret and Collins 2019). Further, we see increased ocean stratification under 4×CO2 (Fig. 15d and Table S7). A more stratified ocean is associated with an increase in both the El Niño events and amplitude in the eastern Pacific (Wang et al. 2020). It can also modify the balance between feedback processes (Dewitte et al.,

2013). Enhanced stratification may also cause negative temperature anomalies in the central to the western Pacific through changes in thermocline tilt (Dewitte et al., 2013). Since the overall ENSO amplitude decreases in our 4xCO2 simulation, we, thus, conclude that the ocean stratification mechanisms cannot be the dominant factor here, but that hf and BJ feedbacks must more than cancel out the effect of ocean stratification on ENSO amplitude.

The increased frequency of extreme El Niño events under 4$\times$CO2 is due to change in the mean position of the ITCZ (Fig. S2), causing frequent reversals of MSSTG (Fig. S3), and eastward extension of the western branch of PWC (Fig. 6), which both result in increased rainfall over the eastern Pacific (see Wang et al. 2020). This is due to greater east equatorial than off-equatorial Pacific warming (see Cai et al. 2020), which shifts the mean position of ITCZ towards the equator (Fig. S2). Simultaneously more rapid warming of the eastern than western equatorial Pacific reduces the ZSSTG, and hence zonal wind stress, as also evident from the weakening and shift of the PWC (Fig. 6) and increased instances of negative ZSSTG anomalies (Fig. S9). Ultimately, this leads to more frequent vigorous convection over the Niño3 region (Fig. 5d), and enhanced rainfall (Fig. 2d, S8). Therefore, despite the weakening of the ENSO amplitude under 4$\times$CO2, rapid warming of the eastern equatorial Pacific causes frequent reversals of meridional and zonal SST gradients, resulting in an increased frequency of extreme El Niño events (see also Cai et al., 2014; Wang et al., 2020).

We note that under GHG forcing, HadCM3L does not simulate an increase in the frequency of extreme La Niña events as found by Cai et al. (2015b) using CMIP5 models. However, it does show an increase in the total number of La Niña events (Table S4). In a multimodel ensemble mean, Cai et al. (2015b) found that the western Pacific warms more rapidly than the central Pacific under increased GHG forcing, resulting in strengthening of the zonal SST gradient between these two regions. Strengthening of this zonal SST gradient and increased vertical upper ocean stratification provide conducive conditions for increased frequency of extreme La Niña events (Cai et al.,

2015b). One reason why we do not see an increase in the frequency of central Pacific extreme La Niña events might be that HadCM3L does not simulate more rapid warming of the western Pacific compared to the central Pacific as noticed by Cai et al. (2015b) (compare our Fig. 1d with Fig. 3b in Cai et al., 2015b), hence, as stronger zonal SST gradient does not develop, across the equatorial Pacific, as needed for extreme La Niña events to occur (see Fig. S9a, c and S10).

4.2 Under solar geoengineering

G1 over cools the upper ocean layers, whereas the GHG-induced warming in the lower ocean layers is not entirely offset, thus increasing ocean stratification (Fig. 15). The increased stratification boosts atmosphere-ocean coupling (see Cai et al., 2018), which favours enhanced westerly wind bursts (Fig. 4a) (e.g., Capotondi et al., 2018) to generate stronger SST anomalies over the eastern Pacific (Wang et al. 2020). The larger cooling of the western Pacific than the eastern Pacific can also enhance westerly wind bursts reinforcing the BJ feedback and hence SST anomalies in the eastern Pacific. We conclude that increased ocean stratification, along with stronger BJ feedback, is the most likely mechanism behind the overall strengthening of ENSO amplitude under G1.

The increased frequency of extreme El Niño events under G1 can be linked to the changes in MSSTG and ZSSTG (see Cai et al., 2014, and Fig. S3, S9). The eastern off-equatorial Pacific cools more than the eastern equatorial regions, providing relatively more conducive conditions for convection to occur through a shift of ITCZ over to the Niño3 region (Fig. 1e). At the same time, the larger cooling of the western equatorial Pacific than of the eastern equatorial Pacific reduces the ZSSTG and convective activity over the western Pacific, which leads to a weakening of the western branch of PWC (Fig. 6e). Hence we see reduced rainfall over the western Pacific and enhanced rainfall from the Niño3 to the central Pacific region (Fig 2e). These mean state changes, strengthening of convection between $\sim$140o W and $\sim$150o E, and more reversals of the MSSTG and ZSSTG (Fig. S3) result in an increased number of extreme El Niño

events in G1 than in piControl (Fig. 7).

In the Discussion and conclusion (see section 5, page 19, lines 1-14), we have added the following paragraph:

To conclude, solar geoengineering can compensate many of the GHG-induced changes in the tropical Pacific, but, importantly, not all of them. In particular, controlling the downward shortwave flux cannot correct one of the climate system's most dominant modes of variability, i.e., ENSO, wholly back to preindustrial conditions. The ENSO feedbacks (Bjerkness and heat flux) and more stratified ocean temperatures may induce ENSO to behave differently under G1 than under piControl and 4×CO2. Different meridional distributions of shortwave and longwave forcings (e.g., Nowack et al., 2016) resulting in the surface ocean overcooling, and residual warming of the deep ocean are the plausible reasons for the solar geoengineered climate not reverting entirely to the preindustrial state. However, we note that this is a single model study, and more studies are needed to show the robustness and model-dependence of any results discussed here, e.g. using long-term multimodel ensembles from GeoMIP6 (Kravitz et al., 2015), once the data are released. The long-term Stratospheric Aerosol Geoengineering Large Ensemble (GLENS; Tilmes et al., 2018) data can also be explored to investigate ENSO variability under geoengineering.

2)

Nonetheless this leads to the question: How large are the differences in mean state and ENSO statistics between G1 and piControl state in comparison to the internal variability in piControl? For example P9, L20-21: the reduction in MSSTG is 9% in G1, is this substantial compared internal variability in piControl and to that seen during an El Nino?

Reply:

We have shown that the 9 % change in MSSTG under G1 is statistically significant (99

% confidence level) relative to piControl using both Bootstrap resampling and a non-parametric Wilcoxon rank-sum test. The increase in the frequency of extreme El Niño events is due to more frequent reversals of MSSTG (Fig. S3 and Table S2). In the revised manuscript, we have tested the change in frequency under both 4×CO2 and G1, relative to piControl, first by using rainfall > 5 mm day-1 as a threshold for extreme El Niño events and then selecting only those events for which rainfall > 5 mm day-1 and MSSTG < 0. Both methods show a statistically significant increase in extreme El Niño events. Choosing extreme events having MSSTG < 0 assures that strong convection has established over the Niño3 region during the extreme. Further, we have shown the histograms of MSSTG for all samples and exclusively for extreme El Niño events, which indicate more frequent reversals of MSSTG both under 4×CO2 and G1 relative to piControl. In the revised manuscript, we have incorporated the following changes:

Overall there is a change in sign and reduction of MSSTG in 4×CO2 (∼-111 %, 99 % cl) and only decrease in G1 (∼-9 %, 99 % cl) (Fig. S3, and Table S2). (See section 3.1.4, page11, lines 17-19)

A threshold of detrended Niño3 total rainfall of 5 mm day-1 recognizes events as extremes even when the MSSTG is positive and stronger, especially under 4×CO2, which plausibly means that ITCZ might not shift over the equator for strong convection to occur during such extremes. The El Niño event of 2015 is a typical example of such events. We test our results with a more strict criterion by choosing only those events as extremes, which have characteristics similar to that of 1982 and 1997 El Niño events (i.e., Niño3 rainfall > 5 mm day-1 and MSSTG < 0). We declare events having characteristics similar to that of the 2015 event as moderate El Niño events (Fig. S5). Based on this method, we find a robust increase in the number of extreme El Niño events both in 4×CO2 (924 %) and G1 (61 %) at 99 % cl. (See section 3.2.2, page14, lines 26-34)

3)

In many of the plots showing differences between experiments and piControl, the con-

fidence level was set to 90%. Given the long time series of the model output, it should be increased to 95% or even 99%. This would perhaps show more regions in G1 where the differences are not significantly different from piControl.

Reply:

All statistics have been recalculated either with a 95 % or 99 % confidence level. See the manuscript with tracked changes.

4)

The conclusion section could provide the reader with a little perspective on whether it is worth it to do the geoengineering solution in the context of projected increase in extreme ENSO activity. A relevant paper to help the discussion: Trenberth KE, Dai A 2007). Geophys Res Lett 34:L15702. doi: 10.1029/2007GL030524

Reply:

In the revised manuscript (see section 5, page 19, lines 1-14), we have included the following paragraphs/statements:

To conclude, solar geoengineering can compensate many of the GHG-induced changes in the tropical Pacific, but, importantly, not all of them. In particular, controlling the downward shortwave flux cannot correct one of the climate system's most dominant modes of variability, i.e., ENSO, wholly back to preindustrial conditions. The ENSO feedbacks (Bjerkness and heat flux) and more stratified ocean temperatures may induce ENSO to behave differently under G1 than under piControl and $4\times$CO2. Different meridional distributions of shortwave and longwave forcings (e.g., Nowack et al., 2016) resulting in the surface ocean overcooling, and residual warming of the deep ocean are the plausible reasons for the solar geoengineered climate not reverting entirely to the preindustrial state. However, we note that this is a single model study, and more studies are needed to show the robustness and model-dependence of any results discussed here, e.g. using long-term multimodel ensembles from GeoMIP6 (Kravitz et

al., 2015), once the data are released. The long-term Stratospheric Aerosol Geoengineering Large Ensemble (GLENS; Tilmes et al., 2018) data can also be explored to investigate ENSO variability under geoengineering.

5)

P11, L36: Picking a result on one model sounds rather odd as we know that the change in ENSO amplitude varies widely across models (e.g., Collins et al. 2010). In a recent study by Cai et al. (2018, Nature, https://www.nature.com/articles/s41586-018-0776-9), however, there seems to be a stronger inter-model agreement on the increase in ENSO amplitude in models that are able to simulate ENSO flavors (see their Extended Data Fig. 8b), as implied in the PC1-PC2 space. So does the HadCM3L model capture the nonlinear relationship between PC1 and PC2 as observed? Here PC1 and PC2 refer to the first and second eigenmodes of tropical Pacific SST (see their Fig. 1). Also, it is relevant to discuss the results of Cai et al. (2018) in 1st paragraph of Page 3.

Reply:

Regarding the change in amplitude, we refer to other studies in the revised manuscript and include the following paragraphs/statements:

Previous studies found that climate models produced mixed responses (both increases and decreases in amplitude) in terms of how ENSO amplitude change with global warming (see Latif et al. 2009; Collins et al. 2010; Vega-Westhoff and Sriver 2017). However, Cai et al. (2018) found an intermodel consensus, for models capable of reproducing ENSO diversity, for strengthening of ENSO amplitude under A2, RCP4.5, and RPC8.5 transient scenarios. (See section 3.2.1, page 13, lines 6-11)

We have included a separate section (2.4) under the title "ENSO representation in HadCM3L" which discusses the HadCM3L capability to simulate ENSO diversity as described by Cai et al. (2018). We have incorporated the following paragraphs/statements in the revised manuscript:

Before employing HadCM3L for studying ENSO variability under 4$\times$CO2, and G1, we evaluate its piControl simulation against present-day observational data. (See section 2.4, page 6, lines 40-41)

Further, we have included the following paragraphs (see section 2.4, page 7, and line 14 to next page line 21):

In addition, we evaluate the ENSO modelled by HadCM3L following a principal component (PC) approach suggested by Cai et al. (2018). Considering distinct eastern and central Pacific ENSO regimes based on Empirical Orthogonal Function (EOF) analysis, they found that climate models capable of reproducing present-day ENSO diversity show a robust increase in eastern Pacific ENSO amplitude in a greenhouse warming scenario. Specifically, the approach assumes that any ENSO event can be represented by performing EOF analysis on monthly SST anomalies and combining the first two principal patterns (Cai et al., 2018). The first two PCs time series, PC1 and PC2, show a non-linear relationship in observational datasets (Fig. S1m). Climate models that do not show such a non-linear relationship cannot satisfactorily reproduce ENSO diversity, and hence are not sufficiently skilful for studying ENSO properties (Cai et al., 2018). Here, we perform EOF analysis on quadratically detrended monthly SST and wind stress anomalies of ERA5 and piControl over a consistent period of 41-year. We evaluate HadCM3L's ability to simulate two distinct ENSO regimes and the non-linear relationship between the first two PCs, i.e., PC2(t) = α[PC1(t)]^2 + β[PC1(t)]^2 + γ (Fig. S1). From ERA5, α = -0.36 (statistically significant at 99 % confidence level, hereafter "cl") whereas in piControl α = -0.31 (99 % cl), which is same as the mean α = -0.31 value calculated by Cai et al. (2018) averaged over five reanalysis datasets. The 1st and 2nd EOF patterns of monthly SST and wind stress anomalies of piControl (Fig. S1 b, e) are comparable with that of ERA5 (Fig. S1 a, d). EOF1 of piControl shows slightly stronger warm anomalies in the eastern equatorial Pacific, whereas negative anomalies over the western Pacific are slightly weaker compared to ERA5. In EOF1, the stronger wind stress anomalies occur to the west of the Niño3 region, which is

a characteristic feature during the eastern Pacific El Niño events (see Kim and Jin 2011a). Compared to ERA5, the spatial pattern of warm eastern Pacific anomalies is slightly stretched westwards, and wind stress anomalies are relatively stronger over the equator and South Pacific Convergence Zone (SPCZ). The 2nd EOF, in both ERA5 and piControl, shows warm SST anomalies over the equatorial central Pacific Niño4 region. The variance distributions for ERA5 and HadCM3L match well for EOF1 (ERA5: 82 %, piContol: 90 %) whereas a large difference exist for EOF2 (ERA5: 18 %, piControl: 10 %).

The PCA is also useful for evaluating how well HadCM3L represents certain types of ENSO events. Eastern and central Pacific ENSO events can be described by an E-Index (PC1-PC2)/$\sqrt{2}$), which emphasizes maximum warm anomalies in the eastern Pacific region, and a C-Index (PC1+PC2)/$\sqrt{2}$) respectively, which focuses on maximum warm anomalies in the central Pacific (Cai et al., 2018). Here, we show the eastern Pacific (EP) Pattern (Fig. S1 g, h) and central Pacific (CP) pattern (Fig. S1 j, k) by linear regression of mean DJF E- and C-Index, respectively, onto mean DJF SST and wind stress anomalies. We find that model's EP and CP patterns agree reasonably well with that of ERA5. HadCM3L underestimates the E-index skewness (1.16) whereas overestimates the C-Index skewness (-0.89) compared to ERA5 (2.08 and -0.58 respectively) averaged over DJF. HadCM3L's performance averaged over the entire simulated period of piControl is also consistent with ERA5 (Fig. S1; α: -0.32, EOF1: 64 %, EOF2, 8%, E-index skewness: 1.30, C-index skewness: -0.42). In general, in HadCM3L, the contrast between the E- and C-index skewness over the entire simulated period is sufficient enough to differentiate relatively strong warm (cold) events in the eastern (central) equatorial Pacific compared to the central (eastern) equatorial Pacific. Finally, we also evaluated the hf and BJ feedbacks which, for piControl, are very similar to those of ERA5 (Table S5-6).

We conclude that HadCM3L has a reasonable skill for studying long-term ENSO variability and its response to solar geoengineering. However, we also highlight the need

for and hope to motivate future modelling studies that will help identify model dependencies in the ENSO response.

We discuss the results of Cai et al. (2018) as follows:

As diagnosed from Sea Surface Temperature (SST) indices in state-of-the-art AOGCMs, there was no intermodel consensus about change in frequency of ENSO events and amplitude in a warming climate (Vega-Westhoff and Sriver 2017; Yang et al., 2018) until Cai et al. (2018) used SST indices based on Principal Component Analysis (PCA). (See section 1, page 2, and line 41 to next page line 4)

However, Cai et al. (2018) later found robust evidence of a consistent increase in El Niño amplitude in the subset of CMIP5 climate models, which were capable of reproducing both eastern and central Pacific ENSO modes. (See section 1, page 3, line 11-14)

Please see Supplementary Fig. S1 and Tables S5-S6 as well.

6)

P7, L10: make clear the results are in *qualitative* agreement with previous studies. Not all of the cited studies are based on 4xCO2.

Reply:

We check our results and categorically mention that our results qualitatively agree with previous studies. Thus we add the following change:

Our SST results under 4xCO2 qualitatively agree with previous studies (Liu et al., 2005; van Oldenborgh et al., 2005; Collins et al., 2010; Vecchi and Wittenberg et al., 2010; Cai et al., 2015a; Huang and Ying et al., 2015; Luo et al., 2015; Kohyama et al., 2017; Nowack et al., 2017). (See section 3.1.1, page 9, line 9-12)

7)

P.7, L13: some studies argue against the use of “El Nino-like” term in describing the mean-state change under greenhouse forcing (e.g., Collins et al. 2010; see also Xie et al. 2010 https://journals.ametsoc.org/doi/10.1175/2009JCLI3329.1). Cautionary is needed to avoid confusions. A relevant reference on the mean state change: diNezio et al https://journals.ametsoc.org/doi/full/10.1175/2009JCLI2982.1.

Reply:

We have deleted the term “El Nino-like” from the revised manuscript and have replaced it with appropriate words like “a significant mean warming” or “a warming state” (See section 1, page 3, lines 18-19; and section 3.1.1 page 8, line 37)

8)

Fig. 2d, e: title of the figure states +0.21 mm/day, -0.23 mm/day. Please explain in the caption that those numbers correspond to the area average difference between experiment and piControl in the tropical Pacific (state domain).

Reply:

The following change is made in the caption of Fig. 1:

The numbers in a-c represent a mean temperature in the corresponding simulation, and numbers in d-e represent an area-averaged difference of piControl with 4$\times$CO2 and G1, respectively, in the tropical Pacific region (25o N-25o S; 90o E-60o W). (See page 28, lines 8-11)

The following change is made in the caption of Fig. 2:

The numbers in a-c represent mean rainfall in the corresponding simulation, and numbers in d-e represent an area-averaged difference of piControl with 4$\times$CO2 and G1, respectively, in the tropical Pacific region (25o N-25o S; 90o E-60o W). (See page 29, lines 7-10)

9)

P9, L22-24: This sentence needs a rework. Avoid the word “observe” on model analysis (models are not observations). I think Wang et al. (2017) was referring to zonal temperature gradient between the maritime continent and central Pacific, not eastern Pacific. The difference is not significant in RCP2.6, but should be significant in RCP8.5 (Cai et al. 2015, Nature Climate Change on extreme La Nina).

Reply:

The use of word “observed” for modelled data has been replaced with appropriate words in the revised manuscript. The reference of Wang et al. (2017) for weakening of ZSSTG has also been removed from the revised manuscript. Instead we add the following statements:

Our results under 4xCO2 are in agreement with Coats and Karnauskas (2017), who using several climate models found a weakening of the ZSSTG under the RCP8.5 scenario.(see section 3.1.4, page 11, line 11-13)

The weakening of the MSSTG is qualitatively in agreement with previous studies under increased GHG forcings (e.g., Cai et al., 2014; Wang et al., 2017). (See section 3.1.4, page 11, lines 21-22)

10)

Fig. 7: Please indicate clearly in the caption that the timeseries have been detrended with non ENSO related trend removed following Cai et al. (2017). Otherwise it would create confusion as other studies show that the 2015/16 Nino3 rainfall is close to the 5 mm/day threshold and is thus classified as an extreme El Nino (Santoso et al. 2017). In panel c, d, it must be rainfall anomalies that are shown because there are negative rainfall values, so wouldn’t the 4 or 3 mm/day threshold be applied here? Panel a and b also have negative rainfall values. Please double check.

Reply:

In the captions, we have added the following text:

Following Cai et al. (2014), a non-ENSO related trend has been removed from the rainfall time series. (See Fig. 7, page 32, lines 8-9; and Fig.S5-S6)

In Fig. 7 and Fig. S5-6, revised manuscript, we have shown total rainfall after subtracting the non-ENSO related trend as described by Cai et al. (2017). In the previous manuscript, we subtracted the non-ENSO related trend, including the intercept term; therefore, negative values were present, and it’s been corrected now.

11)

P12, L28-31: under 4xCO2 the rainfall skewness is dramatically reduced. Does that mean there are less extreme El Nino based on the rainfall definition? If so, this does not seem consistent with the PPE results of Cai et al. (2014) using the same model.

Reply:

In the revised manuscript, we have included the analysis for 4$\times$CO2. We show that extreme El Niño events increase under 4$\times$CO2 using metrics based on rainfall and E-index (See section 3.2.2). The climate regime under 4$\times$CO2 is substantially different from that of piControl (See Fig. S8). The comparison of piControl and 4$\times$CO2 is not simple as mean rainfall, despite zero skewness, significantly shifts to a higher value (9.8 mm day-1) under 4$\times$CO2. We have added the following text in the revised manuscript:

With detrended Niño3 total rainfall exceeding 5 mm day-1 as an extreme, three extreme and seven moderate El Niño events can be identified from the historical record between 1979 and 2017 (Fig. 7a). A statistically significant increase of 526 % (99 % cl) in extreme El Niño events can be seen under 4$\times$CO2 (939 events) relative to piControl (150 events) (Fig. 7b-c). The geoengineering of climate (G1) largely offsets the increase in extreme El Niño frequency under 4$\times$CO2 (Fig. 7d), however, compared to piControl, still a 17 % increase in extremes and a 12 % increase in the total number of El Niño events (moderate plus extreme) can be seen at 95 % cl. Thus, an El Niño event occurring every $\sim$3.3-yr under preindustrial conditions occurs every $\sim$2.9-yr

under solar geoengineered conditions. (See section 3.2.2, page 14, line 17-25)

A threshold of detrended Niño3 total rainfall of 5 mm day-1 recognizes events as extremes even when the MSSTG is positive and stronger, especially under 4×CO2, which plausibly means that ITCZ might not shift over the equator for strong convection to occur during such extremes. The El Niño event of 2015 is a typical example of such events. We test our results with a more strict criterion by choosing only those events as extremes, which have characteristics similar to that of 1982 and 1997 El Niño events (i.e., Niño3 rainfall > 5 mm day-1 and MSSTG < 0). We declare events having characteristics similar to that of the 2015 event as moderate El Niño events (Fig. S5). Based on this method, we find a robust increase in the number of extreme El Niño events both in 4×CO2 (924 %) and G1 (61 %) at 99 % cl. We also performed the same analysis by linearly detrending the rainfall time series and find similar results (Fig. S6). (See section 3.2.2, page 14, line 26-36)

An alternative approach to quantifying extreme El Niño events is based on Niño3 SST index > 1.75 s.d. as an extreme event threshold (Cai et al., 2014). We note that using this definition, no statistically significant change in the number of extreme El Niño events is detected in G1 (61 events), whereas they reduced from 57 in piControl to zero events in 4×CO2 highlighting the dependency of specific results on the precise definition of El Niño events used. However, relative to piControl, Niño3 SST index indicates a statistically significant increase (decrease) of 12 % (46 %) in the frequency of the total number of El Niño events (Niño3 SST index > 0.5 s.d.) (Table S3) in G1 (4×CO2). Further, we examine the change in extreme El Niño events using E-Index > 1.5 s.d. (see Cai et al., 2018) as threshold. The SST based E-Index identifies 79, 147, and 93 extreme El Niño events in piControl, 4×CO2, and G1, respectively. Thus using E-Index, extreme El Niño events increase by 86 % (99 % cl) and 17 % (missing 95 % cl by three events) in 4×CO2 and G1, respectively. Based on the E-index definition, we also see a statistically significant increase in the total number of El Niño events in 4×CO2 (88 %) and G1 (12 %) (Table S3). Note that Wang et al. (2020) showed that

extreme convective events can still happen even if the E-index is not greater than 5 mm day-1 (cf. Figure 2 in Wang et al. 2020). (See section 3.2.2, from page 14, and line 37 to next page line 12)

The increased frequency of extreme El Niño events under 4×CO2 is due to change in the mean position of the ITCZ (Fig. S2), causing frequent reversals of MSSTG (Fig. S3), and eastward extension of the western branch of PWC (Fig. 6), which both result in increased rainfall over the eastern Pacific (see Wang et al. 2020). This is due to greater east equatorial than off-equatorial Pacific warming (see Cai et al. 2020), which shifts the mean position of ITCZ towards the equator (Fig. S2). Simultaneously more rapid warming of the eastern than western equatorial Pacific reduces the ZSSTG, and hence zonal wind stress, as also evident from the weakening and shift of the PWC (Fig. 6) and increased instances of negative ZSSTG anomalies (Fig. S9). Ultimately, this leads to more frequent vigorous convection over the Niño3 region (Fig. 5d), and enhanced rainfall (Fig. 2d, S8). Therefore, despite the weakening of the ENSO amplitude under 4×CO2, rapid warming of the eastern equatorial Pacific causes frequent reversals of meridional and zonal SST gradients, resulting in an increased frequency of extreme El Niño events (see also Cai et al., 2014; Wang et al., 2020). (See section 4.1, page 17, line 24-36)

12)

P13, L28-39: The characterization of extreme La Nina is based on Nino4 (Cai et al. 2015), so it is not clear how Nino3 and Nino3.4 indices are used here to infer changes in extreme La Nina.

Reply:

We have deleted inferences based on Nino3 and Nino3.4 in section 3.2.3 of the revised manuscript.

Figure presentation

13)

Fig. 1e, some areas look white (e.g., eastern equatorial Pacific which is supposed to be approx. -0.2C p7, L9) while the colorbar does not have white on it.

Reply:

We have reproduced Fig. 1e with a different color bar, and visibility of colors has improved in the revised manuscript.

14)

Figure 10: the color limit does not seem correct, which shows much larger values in e, f G1-piControl than the composite anomalies themselves in panels a-d.

Reply:

We have corrected the color limits in Fig. 10.

15)

The colorbar of Fig. 2, right panel especially is not ideal. It is hard to immediately see which are positive or negative without referring to the colorbar.

Reply:

In the revised manuscript, we have reproduced Fig. 2 with a diverging color bar.

16)

Might be best to have the same color scale for comparing the results of 4xCO2 – piControl vs G1 –piControl. This is to convey the message the difference is much smaller for G1 – piControl than for 4xCO2.

Reply:

The differences under G1-piControl are small; if we use the same color bar for 4xCO2-piControl and G1-piControl, most of the information is suppressed for G1-piControl.

Therefore we have used two different color bars.

Minor points

17)

Page 4, L34: that sentence is due to Cai et al. (2014).

Reply:

We have cited Cai et al. (2014) in the revised manuscript. (See section 2.4, page 7, line 2)

18)

P4, L35: delete “the northern part of” – the ITCZ is located north of equator, and that rainfall band moves equatorward during strong El Nino events.

Reply:

We have deleted “the northern part of” in the revised manuscript.

19)

P5, L23: “ggradients”

Reply:

Corrected in the revised manuscript. (See section 2.3, page 5, line 24)

20)

P6, L2: extreme El Ninos are not resulting in just “anomalous rainfall” but unusually large rainfall in the eastern equatorial Pacific.

Reply:

We have deleted the word anomalous and modified the text as follows:

.... Niño3 region resulting in rainfall higher than 5mm day-1 (Cai et al., 2014). (See section 2.3, page 6, lines 1-2)

21)

P6, L 35: “depicts this SSTasymmetry between the western and eastern equatorial Pacific well (Fig. 1a).” – not clear since the observed counterpart is not presented.

Reply:

In the text, we have cited a reference for comparing the piControl SST asymmetry with an observational dataset. We have modified the version as follows:

The piControl simulation (Fig. 1a) reproduces the SST asymmetry between the western and eastern equatorial Pacific well (cf. Fig 1a in Vecchi and Wittenberg 2010). (See section 3.1.1, page 8, lines 34-36)

22)

P8, L10: “problem” – not clear, in what way it is a problem?

Reply:

The word “problem” has been deleted in the revised manuscript. We have modified the text as follows:

That is, while the relative additional rainfall asymmetry between the western and eastern Pacific in 4$\times$CO2 is mostly resolved in G1, the tropical Pacific is overall wetter under 4$\times$CO2 but drier in G1. (See section 3.1.2, page 10, lines 13-15)

23)

P9, L19: repetitive: El Nino being stronger than La Nina already implies asymmetric amplitude.

Reply:

In the revised manuscript, we have modified text as follows:

However, the use of standard deviations to define ENSO amplitude is suboptimal, because amplitudes of El Niño and La Niña events are asymmetric, i.e., in general, El Niño events are stronger than La Niña events (An and Jin 2004; Schopf and Burgman 2006; Ohba and Ueda 2009; Ham 2017). (See section 3.2.1, page 13, lines 22-25)

24)

P9, L29: the shoaling of thermocline is also due to increased stratification associated with surface intensified warming in response to greenhouse forcing.

Reply:

We have added the following text in the revised manuscript:

In 4xCO2, most likely the weakened easterlies (as noticed in Sect. 3.1.3; e.g., Yeh et al., 2009, Wang et al., 2017) and greater ocean temperature stratification due to increased surface warming (see Sect. 4 and Cai et al., 2018) lead to a significant shoaling of the thermocline across the western and central equatorial Pacific. In contrast, relatively little change takes place between 130o W and 90o W. In a CMIP3 multimodel (SRESA1B scenario) ensemble, Yeh et al. (2009) found a more profound deepening of the thermocline in this part of the eastern equatorial Pacific; however, for example, Nowack et al. (2017) did not find such changes under 4xCO2 (cf. their Fig. S9). One possible explanation for this behaviour is the competing effects of upper-ocean warming (which deepens the thermocline) and the weakening of westerly zonal wind stress, causing thermocline shoaling (see Kim et al. 2011a). (See section 3.1.5, from page 11 and line 37 to next page line 8)

25)

P9, L32-36: why not use the maximum of vertical temperature gradient as a proxy of thermocline depth for all scenarios?

Reply:

In the revised manuscript, we have included a map for ocean stratification; we think it can provide some details on this. Further, model ocean vertical resolution (13 levels) is not very high to calculate maximum vertical temperature gradient.

26)

P14, L6-7: for extreme El Nino events, are the PWC, SST, and rainfall anomalies strengthened as well?

Reply:

For extreme El Niño events, the PWC, SST, and rainfall anomalies are weakened. We have rectified the text as follows:

These composites provide process-based evidence for the strengthening (weakening) of extreme La Niña (El Niño) events in G1. We show that the PWC, SST, and composite rainfall anomalies are strengthened for extreme La Niña events, while they are weakened for extreme El Niño events under G1. (See section 3.3, page, 16, lines 5-8)

27)

P14, L23-25: this must be referring to the difference between G1 and piControl. Please make that clear.

Reply:

In the revised manuscript, we have modified text as follows:

During extreme El Niño events, in G1, we find reduced SST (Fig. 9e) and rainfall anomalies (Fig. 10e) over the eastern and western equatorial Pacific with a consistent weakening of the eastern and western branch of PWC (Fig. 11e). (See section 3.3.1, page 16, lines 15-17)

NB. Please see attached Supplementary for figure captions.

Please also note the supplement to this comment:
https://acp.copernicus.org/preprints/acp-2018-1312/acp-2018-1312-AC1-supplement.pdf

Interactive comment on Atmos. Chem. Phys. Discuss., https://doi.org/10.5194/acp-2018-1312, 2019.

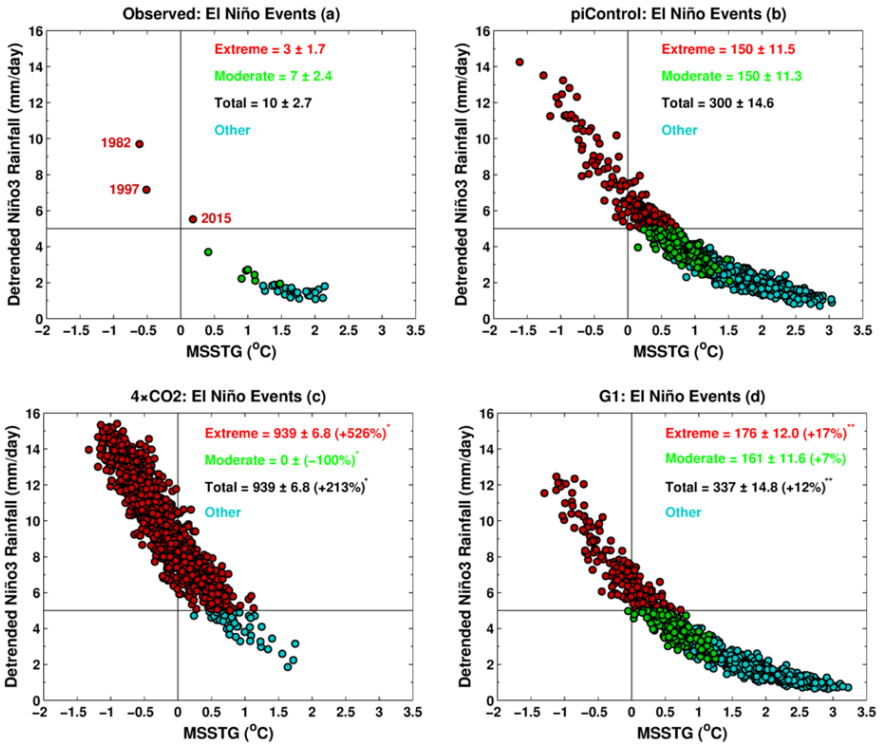

Fig. 1. Figure 7.

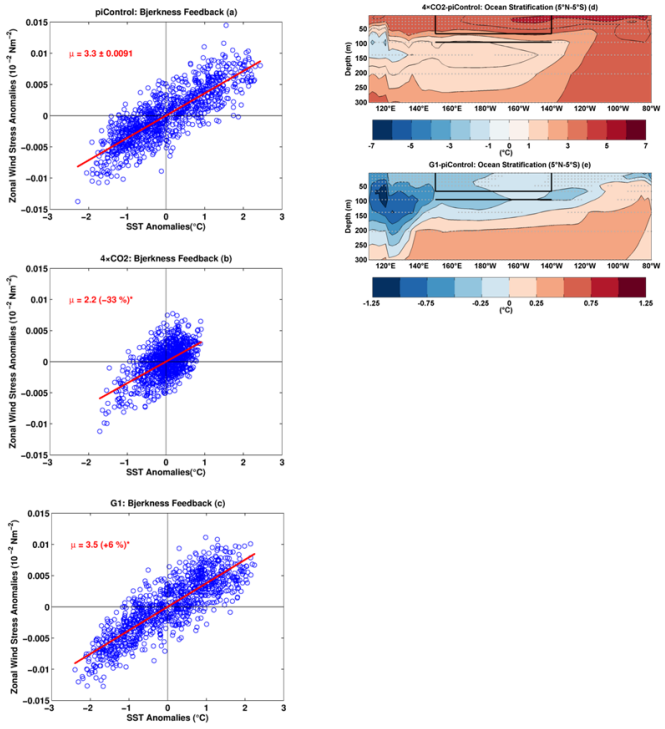

Fig. 2. Figure 15.

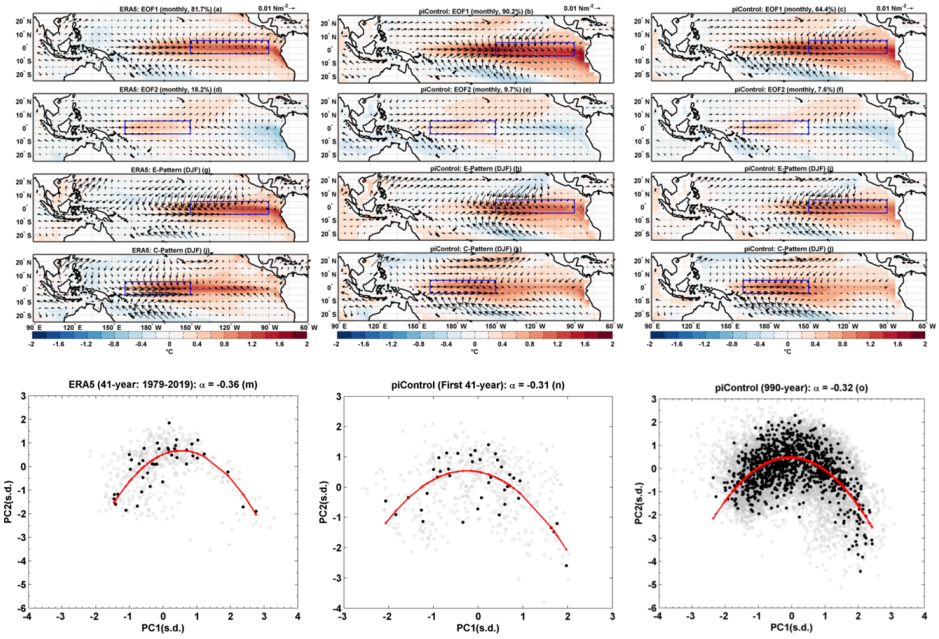

Fig. 3. Figure S1

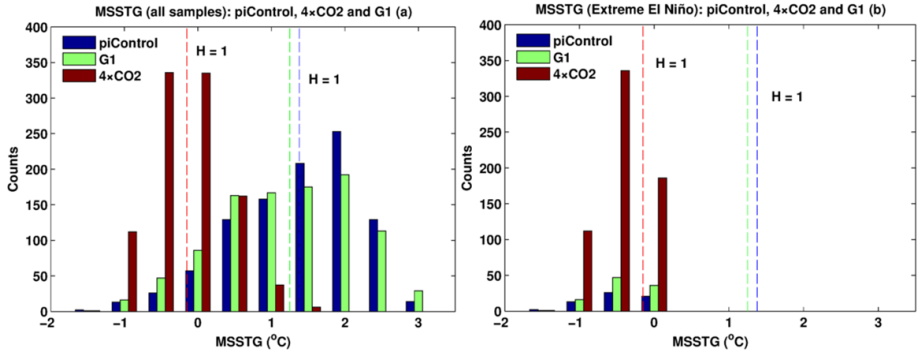

Fig. 4. Figure S3

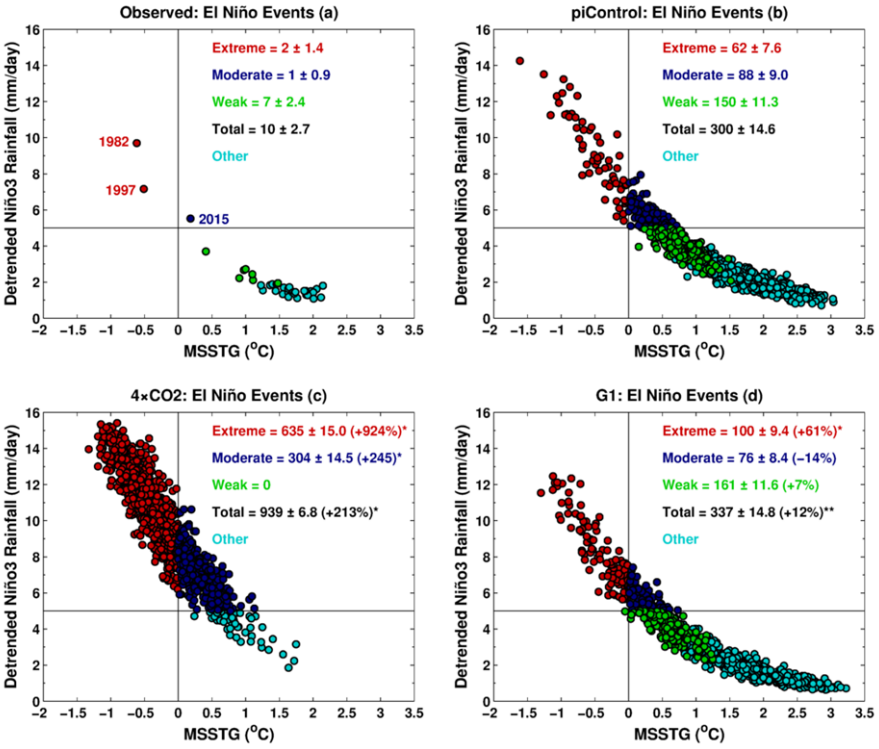

Fig. 5. Figure S5

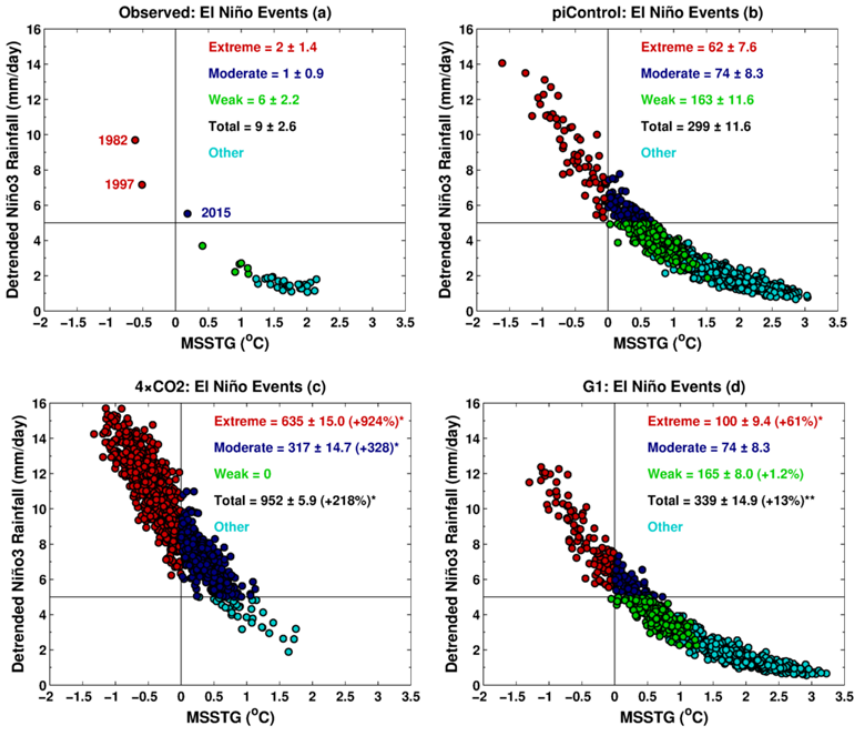

Fig. 6. Figure S6

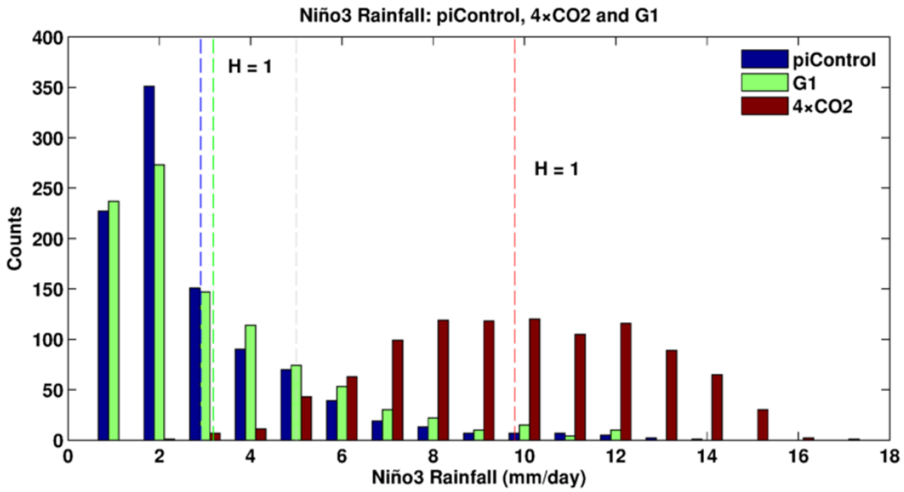

Fig. 7. Figure S8

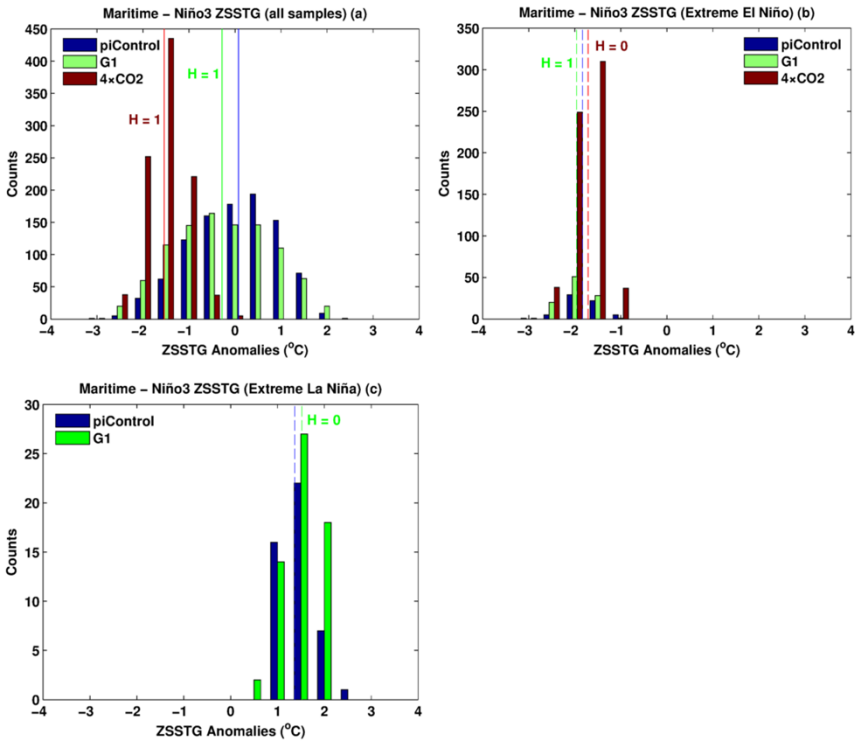

Fig. 8. Figure S9

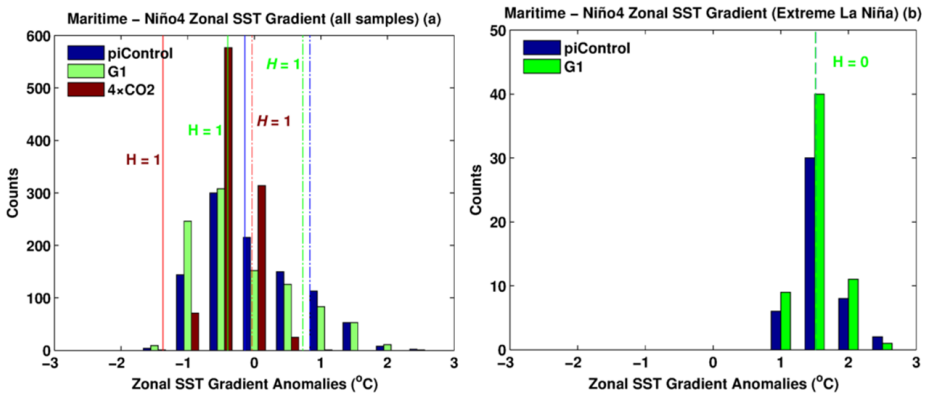

Fig. 9. Figure S10

Table S2. Meridional SST Gradient (MSSTG)

Experiment	Mean (°C)	Difference w.r.t. piControl (°C)	Std. Dev. 10,000 Realizations (°C)	~ Change w.r.t. piControl (%)
piControl	1.38*		0.0265	
4×CO_2	-0.15*	-1.53		-111*
G1	1.25*	-0.13		-9*

Key: *99 % cl; **95 % cl

Fig. 10. Table S2

Table S3. Total number of El Niño events (SST > 0.5 s.d.)

Experiment	No. of Events	Difference w.r.t. piControl	Std. Dev. 10,000 Realizations	~ Change w.r.t. piControl (%)
piControl	300 [300]		14.6 [14.6]	
4×CO_2	161 [565]	139 [265]		-46* [+88*]
G1	337 [337]	37 [37]		+12** [+12**]

Key: Niño3 [E-Index]; *99 % cl; **95 % cl

Fig. 11. Table S3

Table S5. Mean DJF Heat Flux (hf) Feedback

Experiment	hf feedback or Damping Coefficient ($Wm^{-2}/^oC$)	Difference w.r.t. piControl ($Wm^{-2}/^oC$)	Std. Dev. 10,000 Realizations ($Wm^{-2}/^oC$)	~ Change w.r.t. piControl (%)
ERA5	-14.59			
piControl	-14.70		0.52	
4×CO_2	-21.90	+7.19		+48*
G1	-14.85	+0.15		+1.0

*99% cl; **95% cl; Calculation period: ERA5 (41-yrs); HadCM3L (990-yrs)

Fig. 12. Table S5

Table S6. Mean DJF Bjerknes (BJ) Feedback

Experiment	BJ feedback (10^{-2} $Nm^{-2}/^oC$)	Difference w.r.t. piControl (10^{-2} $Nm^{-2}/^oC$)	Std. Dev. 10,000 Realizations ($Wm^{-2}/^oC$)	~ Change w.r.t. piControl (%)
ERA5	3.3			
piControl	3.3		0.0091	
4×CO_2	2.2	-1.1		-33*
G1	3.5	+0.2		+6*

*99% cl; **95% cl; Calculation period: ERA5 (41-yrs); HadCM3L (990-yrs)

Fig. 13. Table S6

Table S7. Mean DJF Ocean Stratification

Experiment	Stratification (^oC)	Difference w.r.t. piControl (^oC)	Std. Dev. 10,000 Realizations (^oC)	~ Change w.r.t. piControl (%)
piControl	2.28*		0.0331	
4×CO_2	5.06*	+2.78		+122*
G1	2.37*	+0.09		+4**

*99% cl; **95% cl

Fig. 14. Table S7